A&A 455, 897–902 (2006)
DOI: 10.1051/0004-6361:20065549

Astronomy & Astrophysics

CO emission from candidate photo-dissociation regions in M 81 *(Research Note)*

J. H. Knapen[1], R. J. Allen[2], H. I. Heaton[3], N. Kuno[4,5], and N. Nakai[6]

[1] Centre for Astrophysics Research, University of Hertfordshire, Hatfield, Herts AL10 9AB, UK
e-mail: j.knapen@star.herts.ac.uk
[2] Space Telescope Science Institute, 3700 San Martin Drive, Baltimore, MD 21218, USA
[3] Johns Hopkins University, Applied Physics Laboratory, Laurel, MD 20723, USA
[4] Nobeyama Radio Observatory, Nobeyama, Minamimaki, Minamisaku, Nagano 384-13, Japan
[5] The Graduate University for Advanced Studies (SOKENDAI), 2-21-1 Osawa, Mitaka, Tokyo 181-0015, Japan
[6] Institute of Physics, University of Tsukuba, Tsukuba, Ibaraki 305-8571, Japan

Received 5 May 2006 / Accepted 5 June 2006

ABSTRACT

Context. At least a fraction of the atomic hydrogen in spiral galaxies is suspected to be the result of molecular hydrogen which has been dissociated by radiation from massive stars.
Aims. In this paper, we extend our earlier set of data from a small region of the Western spiral arm of M 81 with CO observations in order to study the interplay between the radiation field and the molecular and atomic hydrogen.
Methods. We report CO(1–0) observations with the Nobeyama 45 m dish and the Owens Valley interferometer array of selected regions in the Western spiral arm of M 81.
Results. From our Nobeyama data, we detect CO(1–0) emission at several locations, coinciding spatially with H I features near a far-UV source. The levels and widths of the detected CO profiles are consistent with the CO(1–0) emission that can be expected from several large photo-dissociation regions with typical sizes of some 50×150 pc located within our telescope beam. We do not detect emission at other pointings, even though several of those are near far-UV sources and accompanied by bright H I. This non-detection is likely a consequence of the marginal area filling factor of photo-dissociation regions in our observations. We detect no emission in our Owens Valley data, consistent with the low intensity of the CO emission detected in that field by the Nobeyama dish.
Conclusions. We explain the lack of CO(1–0) emission at positions farther from far-UV sources as a consequence of insufficient heating and excitation of the molecular gas at these positions, rather than as an absence of molecular hydrogen.

Key words. galaxies: individual: M 81 – galaxies: ISM – ISM: molecules – ISM: clouds – radio lines: galaxies

1. Introduction

Morphological evidence has been presented on several occasions over the past twenty years that a non-negligible fraction of the atomic gas found in the arms of spiral galaxies may be produced by the destruction of molecular hydrogen in photo-dissociation regions (PDRs) surrounding young massive stars. This view, which was initially developed by comparing the relative placement of dust lanes, H II regions, and H I density enhancements in parts of M 83 (Allen et al. 1985, 1986) and M 51 (Tilanus & Allen 1987), was extensively tested by Allen et al. (1997, hereafter AKBS97) in M 81, based on the relative positions of a large number of far-UV (FUV), Hα, and H I sources. AKBS97 interpreted the morphological information as implying that a significant part of the H I in the spiral arms of M 81 is a product of star formation rather than a precursor to it.

Nevertheless, by conventional measures, the amount of molecular hydrogen in M 81 is not extensive. For example, CO observations from selected regions of M 81, the locations of some of which are indicated in Fig. 1, have been reported by Brouillet et al. (1988), Sage & Westpfahl (1991) and Brouillet et al. (1991, hereafter B91), who find relatively weak CO(1–0) emission from the spiral arms on the basis of relatively low resolution single-dish observations. Taylor & Wilson (1998) reported the detection of resolved emission from three molecular clouds in one of those (Southern) regions with diameters of ∼100 pc, and Brouillet et al. (1998, hereafter B98) describe several clouds that they found interferometrically in one of the (Northern) regions where they had previously detected CO with a single dish. These data indicate that either the earlier hypothesis regarding the origin of H I gas is incorrect for M 81, or there must be a reservoir of (cold) molecular gas that has escaped detection.

We have obtained new single-dish and interferometric measurements in the CO(1–0) line from a region that extends below the southernmost field in the Western arm of M 81 where B91 detected CO emission, to determine whether evidence exists for a non-radiating molecular reservoir. The fields that we observed formed part of our previous study (AKBS97) and contain several candidate PDRs. Although CO gas spanning the H I velocity discontinuity caused by density wave-driven streaming of the gas (e.g., Visser 1980) was not detected from our interferometric observations, we obtained a number of single-dish detections near several H II regions. We ascribe these detections to FUV excitation in the PDRs surrounding several young massive stars, but more spatially resolved data will be required at those sites to confirm this hypothesis. While our results appear to corroborate the absence of molecular gas at or just beyond the spiral arm shock front, we argue that a population of large CO clouds similar to the cold Galactic PDR observed at $l^{\rm II} \approx 216°$ by Williams & Maddalena (1996, hereafter WM96) in the plane of the outer

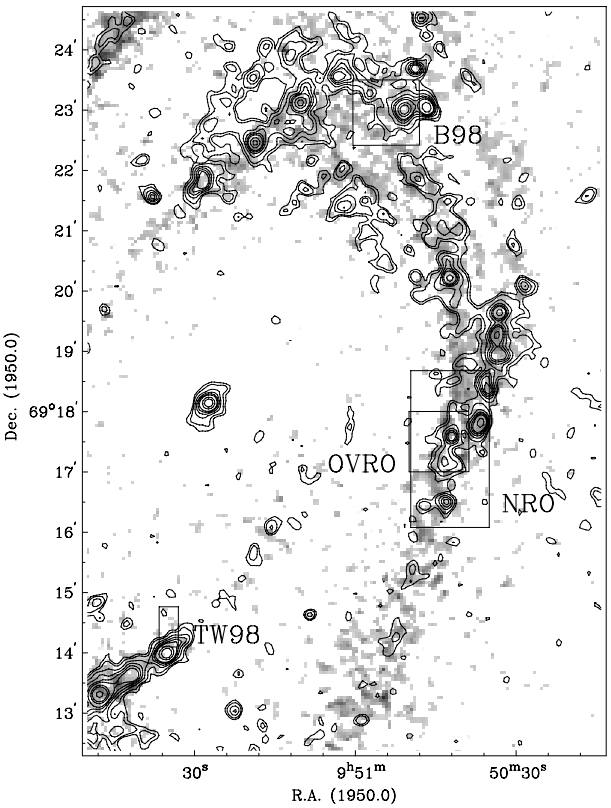

Fig. 1. FUV contours overlaid on a grey-scale representation of the H I integrated intensity map of the Western part of the inner disk of M 81. Overlaid are the fields of our NRO and OVRO observations, as well as the fields observed by Brouillet et al. (1998, labelled B98), and by Taylor & Wilson (1998; labelled TW98). Contour levels for the FUV are 2.3, 3.1, 4.6, 6.2, 7.7, 9.2, 13.9, 18.5 and 36.9×10^{-18} erg cm^{-2} s^{-1} Å^{-1} arcsec^{-2}. Grey levels for the H I vary linearly from 1.5 (light) to 7.3×10^{21} atoms cm^{-2} (dark). FUV and H I data from AKBS97.

Galaxy (i.e., G216−2.5) could exist at that location without being detected at the best synthesised spatial resolution or single-dish sensitivity achieved by our measurements.

2. Empirical modelling of atomic and molecular volume densities

Newly-formed massive stars produce copious amounts of FUV emission. This flux of FUV photons interacts with the surface of the parent molecular cloud and strongly affects its physics and chemistry by heating, dissociating, and exciting the gas (see Hollenbach & Tielens 1999, for an excellent review of the properties of such PDRs). When the presence of a PDR can be confirmed, e.g., from the expected "layered" morphology, useful information can be derived on the physical state of the gas from observations of the spectral lines emitted by the excited atoms and molecules in those regions. Of the many atomic constituents produced by photo-dissociation at and near the surfaces of molecular clouds, atomic hydrogen (H I) is among the easiest to observe.

The PDRs found previously in M 81 by AKBS97 manifest themselves as bright "arcs" and "blisters" of enhanced 21 cm H I emission, located near (and in some cases surrounding) sources of FUV continuum emission. Since the FUV emission is not always accompanied by bright Hα emission, the sources of the dissociating photons must include (and may even be dominated by) B stars. This picture has been developed in more detail by Smith et al. (2000) who isolated 35 candidate PDRs in the giant spiral galaxy M 101 and measured their H I and FUV properties. A simple quantitative model for the H I production in PDRs on the surfaces of molecular clouds was then used to determine the total volume density of the gas in the underlying molecular regions, which was found to lie in the range 30−1000 cm^{-3}, without a radial dependence of the mean value.

The production of H I in PDRs by photodissociation has recently been examined in more detail by Allen et al. (2004, hereafter AHK04) who confirmed the applicability of a simple analytic formula (after some tuning of its parameters) initially proposed by Sternberg (1988). In addition, AHK04 extended the picture to include CO(1–0) emission, which is also produced in the same PDRs by the heating of the ISM (mainly by grains via the photoelectric effect). AHK04 showed that observations of the H I column density and the CO(1–0) line intensity of the same PDR can be combined into a diagnostic which allows one to measure not only the density of the underlying molecular cloud, but also the FUV flux incident upon it. They applied their approach to G216−2.5, and concluded that an incident FUV flux of ∼0.8 (in units of the local FUV flux in the ISM near the sun) was bathing the surface of a large molecular cloud of density ∼200 cm^{-3}, thereby creating the observed levels of H I column density and CO(1–0) surface brightness.

Since the size of the Galactic PDR observed by WM96 (100–200 pc) is of the same order as the linear resolution of the earlier M 81 observations analysed by AKBS97 (∼150 pc), we choose that object as a template for estimating the level of CO(1–0) emission we might expect in our targeted region of the spiral arms of M 81. The total CO(1–0) emission from G216−2.5 is 7.1 K km s^{-1} (as quoted by AHK04), and from Fig. 1 of WM96, we estimate that the total CO(1–0) profile width (*FWHM*) will be about 10 km s^{-1}. From Fig. 2 in WM96, however, we estimate the extent of this CO(1–0) emission to be $\sim 50 \times 150$ pc^2. Since our new single dish detections in M 81 make use of a millimetre radio telescope with an angular resolution of 16 arcsec ≈ 280 pc (1 arcsec = 17.5 pc at the 3.6 Mpc distance we adopted for M 81; Freedman et al. 1994), beam dilution would reduce the expected total emission to ∼0.86 K km s^{-1}.

We have not attempted to compare this extrapolation with predictions from the simple model developed in AHK04 of the integrated CO(1–0) intensity expected near the shock front in M 81 since that model includes photon heating only. The known correlation between the velocity-integrated CO intensity and the nonthermal radio continuum surface brightness in nearby galaxy disks (Adler et al. 1991) and in the Galaxy (Allen 1992) suggests that an enhanced level of cosmic rays also has something to do with heating the ISM, and therefore with elevating the CO surface brightness. The AHK04 model also utilizes the microturbulent velocity width of a single cloud rather than the macroturbulent width typifying an extragalactic ensemble. Nevertheless, the faintness of nonthermal radio continuum emission from M 81 indicates that it is a better choice for assessing the issues under investigation than other nonthermally-bright nearby galaxies such as M 51, M 83, and NGC 6946 because the reduced role of cosmic ray heating provides a more controlled experiment.

3. Observations, data handling, and results

3.1. Nobeyama data

Observations of the ^{12}CO(J = 1–0) emission were made during 1998 January 23 to 26 and March 27 to 31 with the 45 m

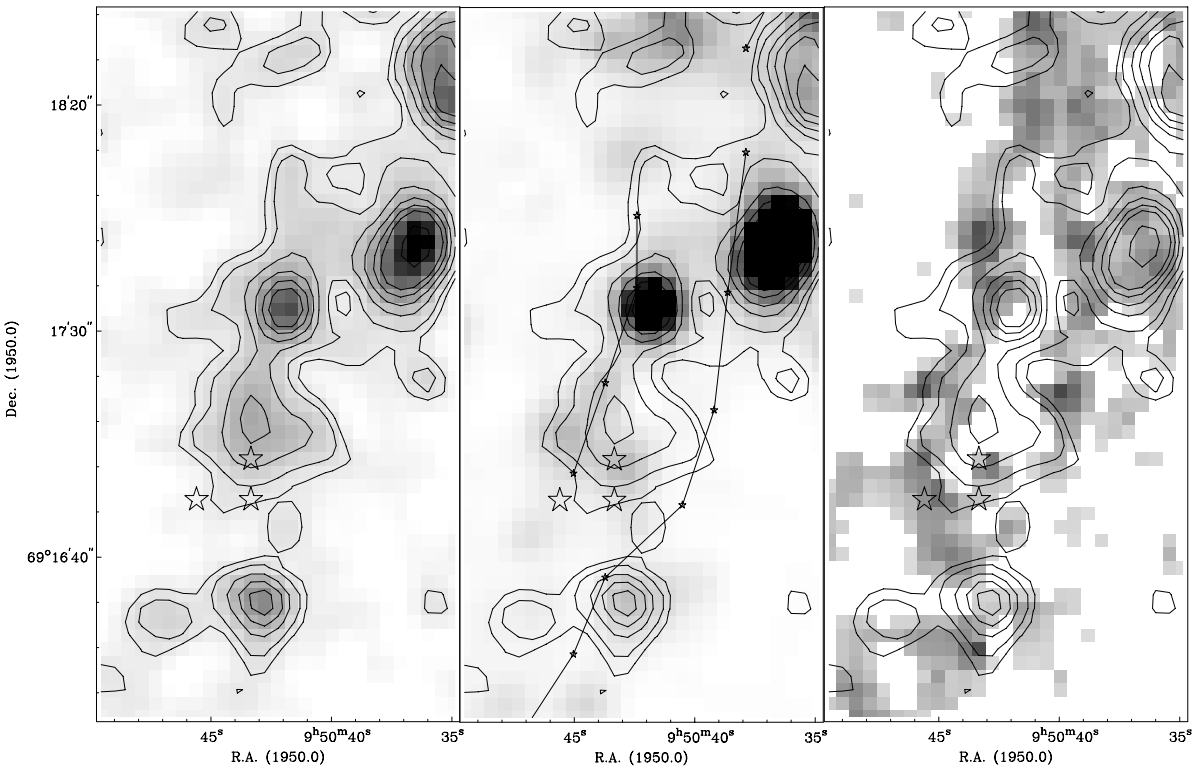

Fig. 2. The region of the spiral arm in M 81 studied in the present paper. Contours in all three panels are of the FUV emission, and contour levels are 2.3, 3.1, 4.6, 6.2, 7.7, 9.2, 13.9, 18.5 and 36.9×10^{-18} erg cm^{-2} s^{-1} Å^{-1} arcsec^{-2}. The contours are overlaid on grey scale representations of the FUV (*left panel*, grey levels from 0.8 [light] to 15×10^{-18} erg cm^{-2} s^{-1} Å^{-1} arcsec^{-2} [dark]); Hα (*middle panel*; grey levels from 0.5 to 95×10^{-17} erg cm^{-2} s^{-1} arcsec^{-2}); and H I (*right panel*, grey levels from 1.5 to 7.3×10^{21} atoms cm^{-2}). The positions of our three most credible CO detections from our NRO observations (B, C, and D in Fig. 3) are indicated in each panel by open star symbols. Centre positions of the dust filaments as measured by Kaufman et al. (1989) are indicated by the line segments drawn in the middle panel.

telescope at the Nobeyama Radio Observatory (NRO). At the rest frequency of the ^{12}CO(1–0) transition (115.271204 GHz), the half-power beam width (HPBW) is 16 arcsec. The aperture and main-beam efficiencies were $\eta_{\rm a} = 0.29$ and $\eta_{\rm mb} = 0.40$, respectively.

We used the 2 × 2 Semiconductor – Insulator – Semiconductor (SIS) focal-plane array receiver which can simultaneously observe four positions separated on the sky by 34 arcsec each (Sunada et al. 1995). Differences in $T_{\rm A}^*$ between the four beams due to the different sideband ratios were adjusted to be equal. We used the SIS single beam receiver with a Martin-Puplett type SSB filter for an image sideband termination at the cryogenic temperature (4 K) to observe selected points effectively. As receiver backends we used 2048 channel wide-band acousto-optical spectrometers (AOS). The frequency resolution and channel spacing were 250 kHz and 125 kHz, respectively. At 115 GHz the corresponding velocity resolution and velocity coverage are 0.65 km s^{-1} and 650 km s^{-1}. Calibration of the line intensity was made by the chopper-wheel method (Ulich & Haas 1976), yielding the antenna temperature $T_{\rm A}^*$ corrected for atmospheric attenuation. In this paper, we use the main beam brightness temperature $T_{\rm mb} \equiv T_{\rm A}^*/\eta_{\rm mb}$ as the intensity scale of the CO brightness temperature. The system noise temperature (SSB), including the atmospheric effect and the antenna ohmic loss, was 500–800 K in $T_{\rm A}^*$, depending on the elevation of the source and the atmospheric conditions. We smoothed the spectra to a velocity resolution of 10 km s^{-1}.

We observed 46 points in a region of about 70 × 90 arcsec. The separation of each point is 11 arcsec in right ascension and declination. The telescope pointing was checked and calibrated every few hours by observing the SiO maser emission of the late-type star R-UMa at 43 GHz. The absolute pointing accuracy was better than 5 arcsec (peak value) throughout the observations.

At the data reduction stage, we checked all individual spectra, with integration times of 20 s, and eliminated those with bad baselines. The remaining spectra were coadded and fitted with a linear baseline.

The region of interest is shown in detail in Fig. 2, where we show the FUV, Hα, and H I distributions at 9 arcsec resolution in the same format as used in AKBS97 for five larger regions of M 81. Dust lanes (based on positions given by Kaufman et al. 1989) are also indicated, in the middle panel. Figure 3 shows the NRO 45 m beam positions overlaid on the grey scale representation of the H I data, as shown in the right panel of Fig. 2. The beam positions designated with letters correspond to detections, as discussed in more detail below, and as tabulated in Table 1.

A sample of the final CO(1–0) spectra is shown in Fig. 4. At most of the 46 positions we did not detect any emission, which corresponds to upper limits ranging from 48 to 201 mK (3σ). We did, however, detect CO emission at some of the positions, which are indicated by letters in Figs. 3 and 4. The H I spectra shown in Fig. 4, derived from a data set kindly made available by Brinks & Walter (2005, private communication), show that in all cases our detected CO emission is at the expected velocity. The most convincing of our detections are labelled B, C, and D ($\gtrsim 5\sigma$ detections in terms of $T_{\rm mb,peak}$; see Table 1). While E also satisfies this 5σ detection criterion, it spans only a single channel in Fig. 4, and is therefore less convincing. The detections B, C, and D are clustered around a weak peak in the FUV

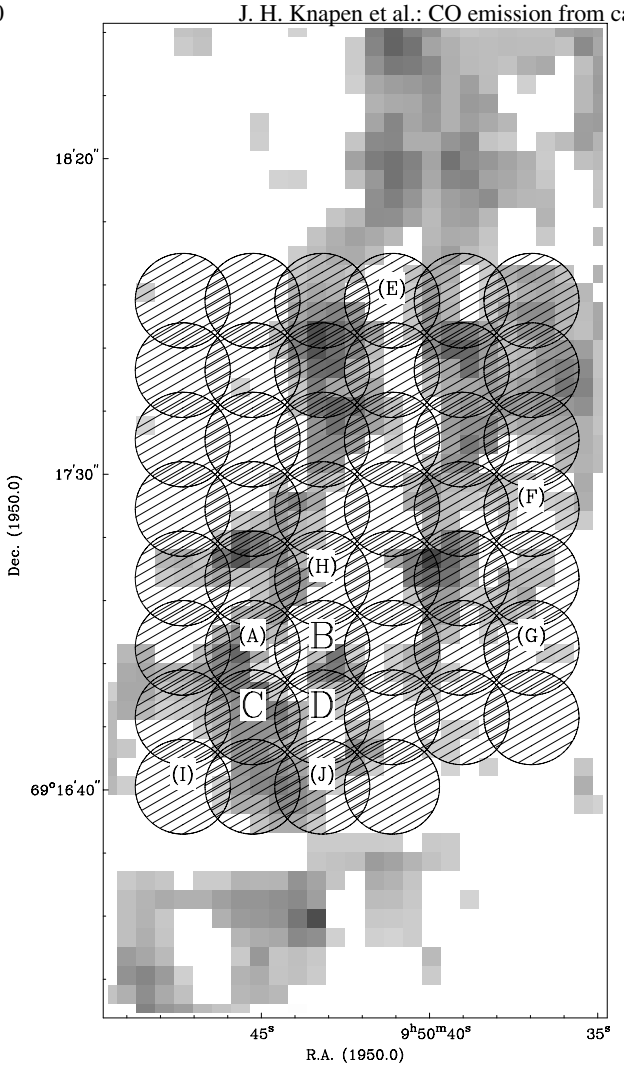

Fig. 3. Positions of the NRO 45 m beam pointings, overlaid on the H I map as shown in the right panel of Fig. 2. Grey levels as in Fig. 2. Letters denote positions where CO was detected (see text); less secure detections are denoted by letters in parentheses.

emission at RA = $09^{h}50^{m}43^{s}$, Dec = 69°17′10″ (B1950.0), and are located close to the H I arc which almost completely surrounds this FUV peak. Around this cluster of detections there are four other, more tentative, detections, where an emission peak is seen at the expected velocity, but with a peak main beam brightness of only $2-4\sigma$ (A, H, I, J). At two further positions, labelled F and G, we detect emission with a peak main beam brightness of $\sim 3\sigma$. Peak antenna temperatures, rms noise levels, and results from Gaussian fits for all the pointings discussed above are summarized in Table 1.

3.2. Owens Valley data

The millimetre array at the Owens Valley Radio Observatory (OVRO) was used on two separate occasions in its low spatial resolution mode to make CO(1–0) observations toward a region in the Western arm of M 81 (see Fig. 1) which corresponds closely to the 1 × 1 arcmin box shown by B91 to the SE of their region N1. The minimum and maximum baselines were 15 m and 115 m during both sessions, corresponding approximately to spatial scales of 620 and 80 pc, respectively, at the adopted distance to M 81. Tracks were obtained on 1998 May 22–23 and 1998 November 5 comprising repetitive cycles of five

Table 1. CO(1–0) measurements obtained using the 45 m NRO dish, $dv = 10\,\mathrm{km\,s^{-1}}$, $T_{\rm mb} = T_{\rm A}^{*}/0.40$. The identification of the measurement, alphabetically as used elsewhere in this paper, and as a position offset from (0,0), which is RA = $09^{h}50^{m}44.0^{s}$, Dec = 69°17′30″ (B1950), is given in Cols. 1 and 2; the integrated intensity in K km s^{-1} is in Col. 3; the peak position and width of the profile, corresponding to velocity and velocity dispersion, are given in Cols. 4 and 5; and the peak main beam temperature is in Col. 6, where the error quoted is the rms of the spectrum (the number in parentheses is the ratio of the two, hence spectrum A is considered a $90/24 = 3.7\sigma$ detection).

Pos.	Offset (″)	$\int T_{\rm mb}\delta v$ (K km s^{-1})	$v_{\rm peak}$ (km s^{-1})	dv (km s^{-1})	$T_{\rm mb,peak}$ (mK)
A	5.5 −27.5	2.32	−6.3	25.3	90 ± 24 (3.7)
B	−5.5 −27.5	2.73	−4.0	18.2	145 ± 23 (6.3)
C	5.5 −38.5	2.52	−14.6	14.7	187 ± 24 (7.8)
D	−5.5 −38.5	1.86	−6.6	15.6	155 ± 32 (4.8)
E	−16.5 27.5	1.20	20.6	7.7	125 ± 24 (5.2)
F	−38.5 −5.5	1.40	20.6	14.3	87 ± 25 (3.5)
G	−38.5 −27.5	1.47	10.5	14.4	85 ± 26 (3.2)
H	−5.5 −16.5	1.07	−9.1	8.6	75 ± 23 (3.3)
I	16.5 −49.5	2.50	−29.0	19.5	100 ± 45 (2.2)
J	−5.5 −49.5	3.19	−38.8	26.4	90 ± 46 (2.0)

separate 5 min integrations on-target and two 5 min integrations on the gain calibrator. Since the phase centre for the target observations was RA = $09^{h}50^{m}44.0^{s}$, Dec = 69°17′30″ (B1950), our 62.9 arcsec primary beam fell nearly completely within the region observed with the NRO dish (Fig. 1).

The digital correlators at Owens Valley were configured to provide two slightly overlapping spectral bands in the upper sideband, each with 32 channels of 1 MHz (2.6 km s^{-1}) width. These bands were subsequently truncated and merged to provide 56 contiguous channels for each track. The data for each track were then merged to produce a dataset with 2480 visibilities corresponding to 13.78 h of on-source integration with a visibility-weighted average system temperature of 989 K. The resulting velocity coverage, centred at −30 km s^{-1} (relative to the local standard of rest), extended from +42.8 to −102.8 km s^{-1}.

All CO mapping was performed with the Astronomical Image Processing System (AIPS) package, using uniform weighting to preserve any extended faint emission in the field. The data were averaged in velocity to obtain a datacube with 28 separate 5.2 km s^{-1} channels. The restoring beam was a Gaussian of width 3.7 × 3.6 arcsec (*FWHM*) at a position angle of 8.2 deg. The flux density noise in the dirty map was 0.032 Jy beam^{-1} (uncorrected for primary beam attenuation) which equates to a temperature noise of 221 mK in the main beam. In addition, the visibilities were tapered to also form a 9 × 9 arcsec beam at a position angle of 46.6 deg for comparison with the H I, Hα, and FUV datasets analysed previously by AKBS97. The noise in the latter (uniformly weighted, uncorrected) dirty map was 0.055 Jy/beam ≡ 62.4 mK. Our resulting maps are 16.4 and 6.7 times more spatially resolved, respectively, than the single dish survey maps made in this region by B91. Since the latter had a sensitivity of $T_{\rm R}^{*} \approx 20$ mK and an on-target observation time of around 0.5 h, equation C2 of AHK04 shows that our new 9 arcsec map has a flux density sensitivity that is approximately 14 times better than the previous survey data.

No clear evidence was obtained for CO emission to the limit of our sensitivity, neither in our 5.2 km s^{-1} channel maps prepared at 3.7 arcsec, nor in those at 9 arcsec resolution. While several features appear on each map, the number of features with

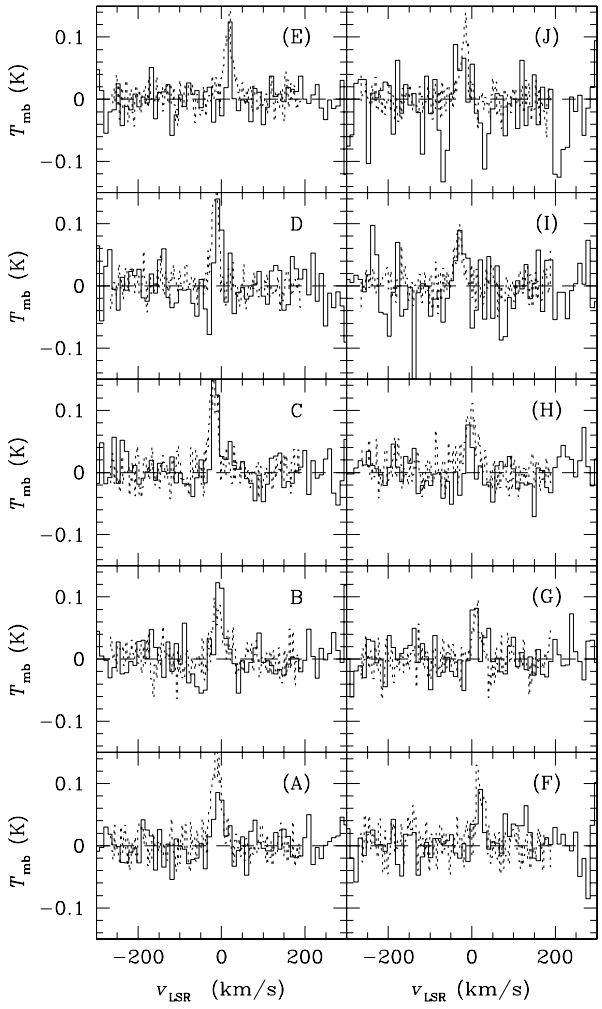

Fig. 4. Final CO(1–0) spectra from NRO (drawn lines), smoothed to dv = 10 km s^{-1} velocity resolution. Letters in this figure correspond to positions of the telescope pointing as shown in Table 1 and Fig. 3, with the (0,0) offset corresponding to position RA = 09^{h}50^{m}44.0^{s}, Dec = 69°17′30″ (B1950). They indicate spectra discussed in more detail in the paper; less secure detections are denoted by letters in parentheses. The dotted lines indicate H I spectra, on an arbitrary scale, at the same position.

positive flux density exceeding preset thresholds roughly equals the number of negative-valued threshold crossings. When the smoothed (9 arcsec) flux density maps were filtered at 3σ, no features repeated from one channel map to the next.

To further quantify these results, we have derived an upper limit to the CO(1–0) flux density from this region based on noise estimates made with the AIPS task IMSTAT, which were derived by fitting Gaussian functions to pixel histograms. The corresponding 3σ upper limit to the flux density value is 163.8 mJy beam^{-1}. Accordingly, the velocity-integrated 3σ upper limit in our field is (163.8 mJy beam^{-1}) × (2 × 10^{6} Hz) = 3.276 × 10^{5} (Jy beam^{-1}) Hz over the 2-channel span corresponding to our chosen velocity resolution. This corresponds to 0.85 Jy km s^{-1} or 1.03 K km s^{-1} for our 9 arcsec beam. Although several of our strongest detections at NRO had integrated intensities greater than this level, only NRO pointings E, H, and part of B fell within our primary beam at Owens Valley. The integrated intensities from E and H are near our OVRO sensitivity limit, and B is on the periphery of the primary OVRO beam.

4. Discussion

The results described in the previous section from the large dish at Nobeyama have extended the regions where CO has been found in the Western arm of M 81 to locations that are farther down that feature than the southernmost field detected by B91. While interesting in itself, the central issue in interpreting this result is: why did the emission stop there? The two most plausible explanations are that the lack of CO(1–0) emission indicates the absence of measurable quantities of molecular gas in dark regions of the observed field, or that the field contains low density gas that isn't heated sufficiently to reveal its presence radiatively. The first interpretation is a consequence of the prevailing view that the CO(1–0) surface brightness and the column density of molecular hydrogen are linearly related, independent of any effects caused by localised heating (Young & Scoville 1991; Combes 1991). In this case, the H I ridge observed downstream from the velocity shock front probably represents the compression of previously existing atomic gas (Kaufman et al. 1989).

An alternative explanation that is consistent with our observations is that the low flux of cosmic rays and the low FUV surface brightness are inadequate to sufficiently heat the ISM to shine in the CO(1–0) line in most of our field. A low cosmic ray flux is implied by the faint levels of nonthermal radio continuum emission from M 81, and low FUV levels are evident in many regions of Figure 2. Emission is observed in areas where heating by photons through the photoelectric effect, and by cosmic rays through ionisation, leads to a rise in the kinetic temperature to a level sufficient, along with the density, to allow the radiating CO energy levels to be populated.

To illustrate these points, we note that the cosmic ray intensity appropriate for the Galaxy in the neighbourhood of the Sun would heat giant molecular clouds (GMCs) that are just dense enough to have thermalized CO emission ($n \approx 10^4$ cm^{-3}) only to ∼5 K (Tielens 2005, p. 352). This is much lower than is observed in localized regions of GMCs in the Galaxy. At densities below ∼10^3 the CO level populations would be subthermally excited, leading to even lower radiation temperatures. As justification for comparing M 81 with the Milky Way, we note that the radio continuum surface brightness, which can be used as a proxy for the cosmic ray flux, is similar in the disks of our Galaxy and M 81, at a level that is an order of magnitude lower than that in M 51 (Adler et al. 1991; Allen 1992).

We can readily draw two conclusions from this discussion. First, regions showing high-temperature CO emission must be heated by a supplementary source in addition to cosmic rays – this source is most likely photoelectric heating of the gas caused by dust absorption of FUV photons, although in some cases H_2 formation heating may play a role (Röllig et al. 2006). In Galactic GMCs, such sources can usually be easily identified as nearby recently-formed massive O/B stars. Second, in the absence of such photons and a sufficient level of cosmic ray flux, the cooling in GMCs is so efficient that the kinetic temperature will quickly fall below 5 K, making the detection in any *emission* line tracer virtually impossible. This, we postulate, is what happens in M 81.

The lack of CO emission at locations between the H I velocity shock and the atomic hydrogen ridge, and its weak detection near several H II regions downstream from the shock, is consistent with the interpretation by Allen et al. (1985, 1986) and Tilanus & Allen (1987) of morphological data from M 83 and M 51, i.e., that the interstellar gas remains primarily molecular after passing through the shock until it dissociates in the neighbourhood of giant H II region complexes downstream. The

spatial extent of our observations is more than adequate to search for such patterns. Since one arcsec corresponds to ∼17.5 pc at the 3.6 Mpc distance assumed for M 81, our 63 arcsec OVRO field alone spans nearly 1.1 kpc. This is more than twice the separation claimed by Kaufman et al. (1989) for the distance between the H I velocity shock and the atomic hydrogen ridge in the Western arm of the latter galaxy.

The cold Galactic cloud described by WM96, G216−2.5, provides a useful template for what we might observe from low density gas clouds in M 81. Although AHK04 found that the most likely density for this cloud was 200 cm^{-3}, the uncertainty in that determination was large enough to render the role of collisional excitation uncertain. Since the beam-diluted integrated intensity of this PDR at the distance of M 81 would be ∼0.9 K km s^{-1} when observed by the 16 arcsec NRO beam, similarly excited clouds with similar profile widths (∼10 km s^{-1}, cf. Sect. 2) should be apparent in our observations. The three firm detections found earlier (i.e., B, C, and D) are all somewhat brighter (by a factor of 2–3) and broader (by a factor of ∼1.5) than this estimate, perhaps indicating the presence of multiple PDR structures at these positions.

The absence of CO emission in our single beam fields that cover the region between the velocity front and the H I ridge sets an upper limit of ∼0.8 K km s^{-1} for the integrated intensity of the gas from that region. If low density molecular gas does reside there, it is not excited sufficiently by the low FUV flux to be detected at the best sensitivity we achieved. The lack of emission at more strongly irradiated locations along the H I ridges in Fig. 3 could easily be caused by enhanced beam dilution from structures that are smaller in linear size than the WM96 cloud. The WM96 cloud would have a beam-diluted integrated intensity ∼2.7 K km s^{-1} in our 9 arcsec synthesized OVRO beam at the distance of M 81. Although this exceeds the 3σ sensitivity value determined for that array by a factor of ∼2.6, the pointings detected by the Nobeyama telescope only partially fell within the OVRO field.

To test the consistency of our findings with earlier results, and the plausibility of using the WM96 PDR as a template for modelling putative undetected gas clouds in our region of the Western arm, we reinterpret the results obtained by B98 with the IRAM Plateau de Bure interferometer. The location of their field is shown in our Fig. 1, while the resulting CO(1–0) map appears in Fig. 1 of their paper. From the extent and maximum intensity of the structures shown in their figure, we estimate that the NRO 45 m beam would have reported a brightness of only ∼0.4 K km s^{-1} for their region C3. The combination of regions C1 and C2, which could fall into one of our beams, would have an integrated intensity of about 1 K km s^{-1}. Thus, we would not have detected clouds in our area with the characteristics found by B98 for C3, while the combination of clouds C1 and C2 would have yielded only a marginal detection. None of these clouds would have been detected at the 3σ level in our 9 arcsec OVRO maps.

When we compare the extrapolated properties of the G216−2.5 PDR with the earlier CO results from B98, it is clear that they have similar CO brightnesses (∼0.8 K km s^{-1} for the latter) and sizes (50 × 100 pc for the WM96 cloud, and at most 150−250 pc for the B98 clouds). The general lack of CO detections in the area observed with the NRO dish is entirely consistent with this picture: we detect a few stronger peaks, but fail to detect CO at the majority of our pointings. This is exactly what we would expect to see if we had observed clouds in our region that were similar to those found by B98 in their field: a marginal detection from C1+C2, and no detections elsewhere in the field. We thus ascribe our lack of CO detections to being predominantly a filling factor effect – individual CO-emitting regions may be relatively bright, but in our 16 arcsec NRO beam they would be diluted to below the detection threshold.

5. Conclusions

We have detected CO(1–0) emission at several locations showing bright H I features near FUV sources in M 81. The levels and widths of the detected CO profiles are consistent with the CO(1–0) emission to be expected from several large photo-dissociation regions with typical sizes of ∼50 × 150 pc located within our NRO beam of size 280 pc. Non-detections, either at other pointings near FUV sources that contain bright H I, or in our synthesized maps, are likely to be a consequence of the marginal area filling factors of PDRs in our observations, and future surveys should be prepared to substantially increase the sensitivity and spatial resolution over what we have achieved here. The lack of CO(1–0) emission at positions farther from the sources of FUV is consistent with insufficient heating of the ISM, resulting in insufficient excitation of the CO molecules.

Acknowledgements. We thank Dr. N. Brouillet for providing a CO sensitivity estimate germane to the undetected field just to the South-East of their field N1, and Prof. E. Brinks and Dr. F. Walter for providing access to unpublished H I data of M 81. R.J.A. is grateful to Prof. J. H. Hough at the University of Hertfordshire and Dr. S. Beckwith at the Space Telescope Science Institute for their generous travel support in connection with the completion of this paper. J.H.K. wishes to acknowledge the Leverhulme Trust for the award of a Leverhulme Research Fellowship, as well as the hospitality of our Japanese colleagues during his visit to Nobeyama.

References

Adler, D. S., Allen, R. J., & Lo, K. Y. 1991, ApJ, 382, 475
Allen, R. J. 1992, ApJ, 399, 573
Allen, R. J., Atherton, P. D., & Tilanus, R. P. J. 1985, in Birth and Evolution of Massive Stars and Stellar Groups, ed. W. Boland, & H. van Woerden (Dordrecht: Reidel), 243
Allen, R. J., Atherton, P. D., & Tilanus, R. P. J. 1986, Nature, 319, 296
Allen, R. J., Knapen, J. H., Bohlin, R., & Stecher, T. P. 1997, ApJ, 487, 171 (AKBS97)
Allen, R. J., Heaton, H. I., & Kaufman, M. J. 2004, ApJ, 608, 314 (AHK04)
Brouillet, N., Baudry, A., & Combes, F. 1988, A&A, 196, L17
Brouillet, N., Baudry, A., Combes, F., Kaufman, M., & Bash, F. 1991, A&A, 242, 35 (B91)
Brouillet, N., Kaufman, M., Combes, F., Baudry, A., & Bash, F. 1998, A&A, 333, 92 (B98)
Combes, F. 1991, ARA&A, 29, 195
Freedman, W. L., Hughes, S. M., Madore, B. F., et al. 1994, ApJ, 427, 628
Hollenbach, D. J., & Tielens, A. G. G. M. 1999, Rev. Mod. Phys., 71, 173
Kaufman, M., Elmegreen, D. M., & Bash, F. N. 1989a, ApJ, 345, 697
Kaufman, M., Bash, F. N., Hine, B., et al. 1989b, ApJ, 345, 674
Röllig, M., Ossenkopf, V., Jeyakumar, S., Stutzki, J., & Sternberg, A. 2006, A&A, 451, 917
Sage, L. J., & Westpfahl, D. J. 1991, A&A, 242, 371
Smith, D. A., Allen, R. J., Bohlin, R. C., Nicholson, N., & Stecher, T. P. 2000, ApJ, 538, 608
Sternberg, A. 1988, ApJ, 332, 400
Sunada, K., Noguchi, T., Tsuboi, M., & Inatani, J. 1995, ASP Conf. Ser., 75, 230
Taylor, C. L., & Wilson, C. D. 1998, ApJ, 494, 581
Tielens, A. G. G. M. 2005, The Physics and Chemistry of the Interstellar Medium (Cambridge: Cambridge University Press)
Tilanus, R. P. J., & Allen, R. J. 1987, in Star Formation in Galaxies, ed. C. J. Lonsdale Persson (NASA Conf. Pub. 2466), 309
Ulich, B. L., & Haas, R. W. 1976, ApJS, 30, 247
Visser, H. C. D. 1980, A&A, 88, 159
Williams, J. P., & Maddalena, R. J. 1996, ApJ, 464, 247 (WM96)
Young, J. S., & Scoville, N. Z. 1991, ARA&A, 29, 581